PNAS
www.pnas.org

Supplementary Information for

Altered CXCR4 dynamics at the cell membrane impairs directed cell migration in WHIM syndrome patients.

Eva M. García-Cuesta[1], José Miguel Rodríguez-Frade[1], Sofía R. Gardeta[1,2], Gianluca D'Agostino[1], Pablo Martínez[1], Blanca Soler Palacios[1], Graciela Cascio[3], Tobias Wolf[4], Nicolas Mateos[5], Rosa Ayala-Bueno[1], César A. Santiago[6] , Pilar Lucas[1], Lucia Llorente[7], Luis M. Allende[7], Luis Ignacio González-Granado[7,8], Noa Martín-Cófreces[9,10,11], Pedro Roda-Navarro[7,12], Federica Sallusto[4,13], Francisco Sánchez-Madrid[9,10,11], María F. García-Parajo[4,14], Laura Martínez-Muñoz[15,16], Mario Mellado[1]*

[1] Chemokine Signaling group, Department of Immunology and Oncology, Centro Nacional de Biotecnología/CSIC, Campus de Cantoblanco, E-28049, Madrid, Spain

[2] Department of Molecular Biosciences, Universidad Autónoma de Madrid, E-28049, Madrid, Spain

[3] Meyer Cancer Center, Weill Cornell Medicine, New York, NY 10021

[4] Institute of Microbiology, ETH Zürich; Zürich, Switzerland.

[5] ICFO-Institut de Ciencies Fotoniques, The Barcelona Institute of Science and Technology, E-08860 Barcelona, Spain

[6] X-ray Crystallography Unit, Centro Nacional de Biotecnología/CSIC, Campus de Cantoblanco, E-28049, Madrid, Spain

[7] 12 de Octubre Health Research Institute (imas12), E-28012, Madrid, Spain.

[8] Department of Public Health School of Medicine, School of Medicine Universidad Complutense de Madrid, E-28040, Madrid, Spain

[9] Immunology Service, Hospital Universitario de la Princesa, UAM, IIS-IP. E-28006, Madrid, Spain.

[10] Area of Vascular Pathophysiology, Laboratory of Intercellular Communication, Fundación Centro Nacional de Investigaciones Cardiovasculares-Carlos III, E-28029, Madrid, Spain.

[11] Centro de Investigación Básica en Red cardiovascular, CIBERCV, E-28029, Madrid, Spain.

[12] Department of Immunology, Ophthalmology and ENT, School of Medicine, Universidad Complutense de Madrid, E-28040, Madrid, Spain

[13] Institute for Research in Biomedicine, Bellinzona, Università della Svizzera italiana, Lugano, Switzerland

[14] ICREA- Pg. LLuis Campanys 23, E-08010, Barcelona, Spain

[15] Department of Cell Signaling, Centro Andaluz de Biología Molecular y Medicina Regenerativa/CSIC, E-41092, Sevilla, Spain

[16] Department of Medical Biochemistry, Molecular Biology and Immunology, University of Sevilla, Medical School, E-41004, Sevilla, Spain

*Mario Mellado

Email: mmellado@cnb.csic.es

This PDF file includes:

Figures S1 to S4

Legends for Movies S1 to S16

Supplementary methods

References

Other supplementary materials for this manuscript include the following:

Movies S1 to S16

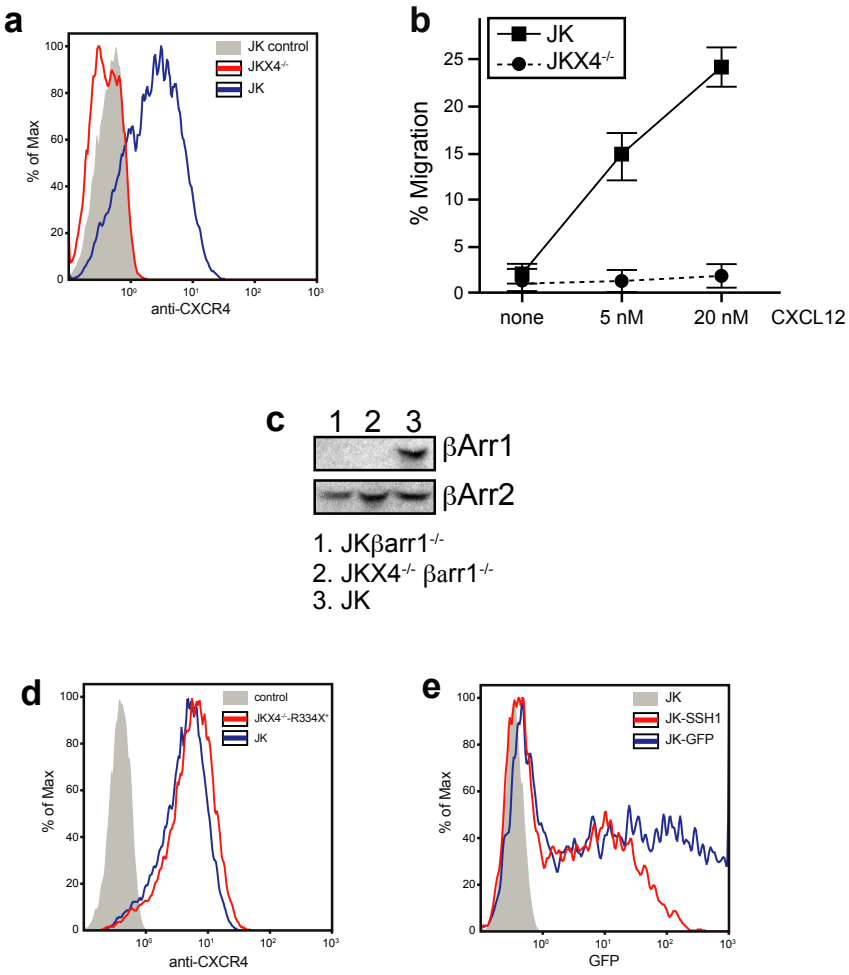

Fig. S1. Characterization of cell lines used in the study. (a) CXCR4 receptor levels in Jurkat (JK) and JKX4$^{-/-}$ cells analyzed by flow cytometry using an anti-CXCR4 antibody. **(b)** JK and JKX4$^{-/-}$ cell migration in Boyden chambers in response to CXCL12. Data are shown as the mean percentage (plus SD) of input cells that migrate (n = 3). **(c)** Expression of βarrestins 1 and 2 in JK, JKβarr1$^{-/-}$ and JKX4$^{-/-}$βarr1$^{-/-}$ cells analyzed by western blotting with specific antibodies. **(d)** CXCR4 receptor levels in JK and JKX4$^{-/-}$R334X^{+} cells analyzed by flow cytometry using an anti-CXCR4 antibody. **(e)** Flow cytometry analysis of GFP expression in JK cells transiently transfected with GFP-SSH1 (JK-SSH1) or GFP alone (JK-GFP).

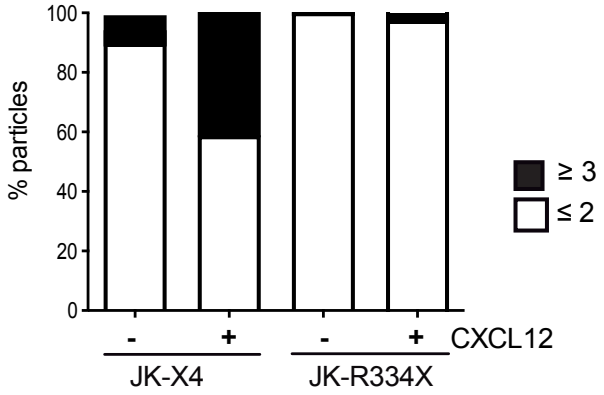

Fig. S2. Receptor distribution under heterozygous conditions. SPT analysis of CXCR4^{R334X}-AcGFP (-R334X) and CXCR4-AcGFP (-X4) in transiently transfected Jurkat (JK) cells on fibronectin (FN) or on FN+CXCL12-coated coverslips. Frequency of CXCR4-AcGFP and CXCR4^{R334X}-AcGFP particles expressing the same number of receptors [monomers and dimers (≤ 2) or bigger nanoclusters (≥ 3)] in JK cells, calculated from mean spot intensity (MSI) values of each particle using as reference the MSI value of monomeric CD86-AcGFP (909 particles in 29 cells on FN; 1065 in 18 cells on FN+CXCL12 in JK-X4 cells; 663 in 31 cells on FN; 674 in 35 cells on FN+CXCL12 in JK-R334X cells; [n = 3]).

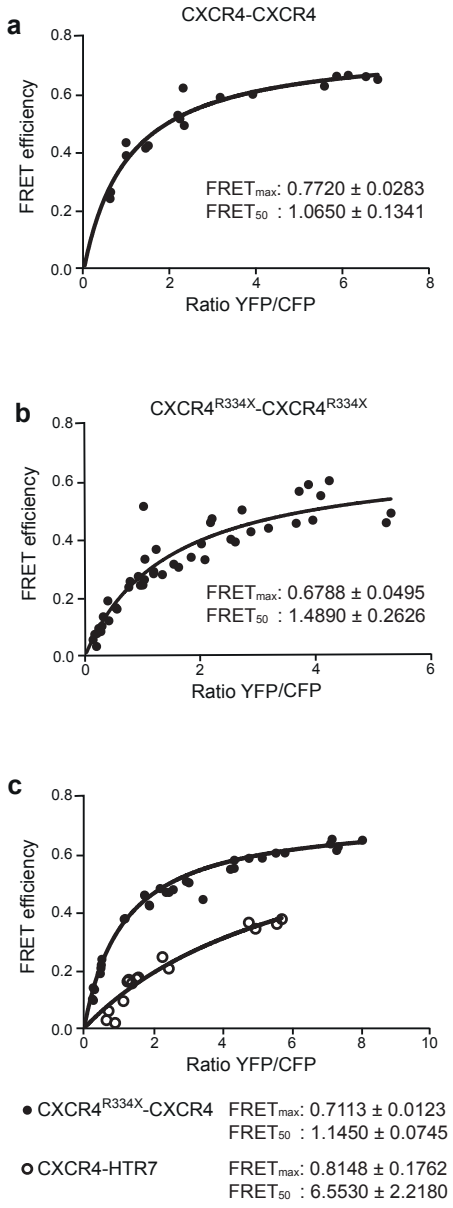

Fig. S3. CXCR4 and CXCR4^{R334X} form homo- and heterodimers. FRET saturation curves for **(a)** CXCR4/CXCR4, **(b)** CXCR4^{R334X}/CXCR4^{R334X} and **(c)** CXCR4^{R334X}/CXCR4 complexes in living cells. Curves were obtained using HEK-293T cells transiently cotransfected with either **(a)** the vector encoding CXCR4-CFP plasmid (2 μg, ~754199 FU) and increasing amounts of CXCR4-YFP plasmid (350176–2319764 FU) or **(b)** CXCR4^{R334X}-CFP (2 μg, ~735842 FU) and increasing amounts of CXCR4^{R334X} -YFP plasmid (180359–2423623 FU). **(c)** For heterodimer evaluation, we

used CXCR4^{R334X}-CFP plasmid (2 μg, ~1103424 FU) and increasing amounts of CXCR4-YFP plasmid (607636–5217397 FU). For negative control **(c)**, cells were transfected with CXCR4-CFP (2 μg, ~1148952 FU) and increasing amounts of HTR7-YFP plasmid (201384–713466 FU). Values represent mean ± SEM (n = 3 in duplicate). $FRET_{50}$ and $FRET_{max}$ values (mean ± SEM) were calculated according to a nonlinear regression equation applied to a single binding-site model (n = 3) (ND, not determined).

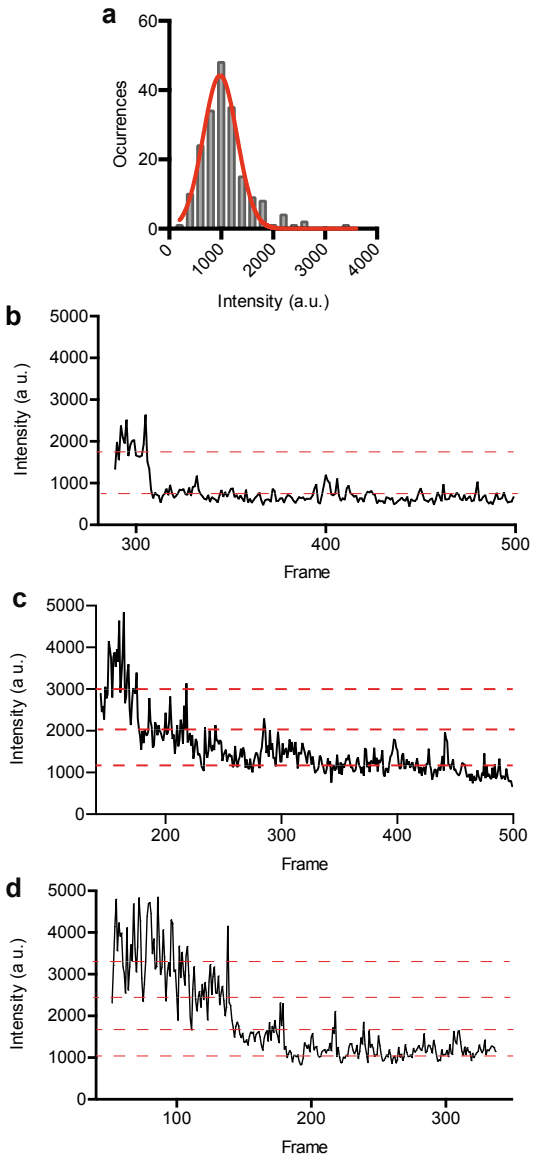

Fig. S4. Characterization and calculation of reference parameters for particles diffusion and intensity. **(a)** Fluorescence intensity histogram from monomeric CD86-AcGFP single particles, detected by one photobleaching step evaluation (data from 193 trajectories in 74 cells in 3-5 separate experiments). The reference fluorescence intensity value for monomer (980 ± 86 a.u.) was obtained from the Gaussian fit (red line) of the histogram. **(b-d)** Representative one-, two- and multi-step photobleaching of CXCR4-AcGFP trajectories.

Movie S1 (separate file).

Related to Figure 3. Representative movie of CXCR4-AcGFP on live JKX4$^{-/-}$ cells captured by SPT-TIRF, showing the diffusion of CXCR4 particles (monomers, dimers, and nanoclusters) at steady state (FN). The video was acquired and displayed at 10 frames/s.

Movie S2 (separate file)

Related to Figure 3. Representative movie of CXCR4-AcGFP on live JKX4$^{-/-}$ cells captured by SPT-TIRF, showing the diffusion of CXCR4 particles (monomers, dimers, and nanoclusters) after CXCL12 stimulus. The video was acquired and displayed at 10 frames/s.

Movie S3 (separate file)

Related to Figure 3. Representative movie of CXCR4^{R334X}-AcGFP on live JKX4$^{-/-}$ cells captured by SPT-TIRF, showing the diffusion of CXCR4^{R334X} particles (monomers, dimers, and nanoclusters) at steady state (FN). The video was acquired and displayed at 10 frames/s.

Movie S4 (separate file)

Related to Figure 3. Representative movie of CXCR4^{R334X}-AcGFP on live JKX4$^{-/-}$ cells captured by SPT-TIRF, showing the diffusion of CXCR4^{R334X} particles (monomers, dimers, and nanoclusters) after CXCL12 stimulus. The video was acquired and displayed at 10 frames/s.

Movie S5 (separate file)

Related to Figure 4. Representative video of JKX4$^{-/-}$-X4 cell migration on fibronectin-coated μ-Slide Chemotaxis chambers in the absence of a CXCL12 gradient. Images over time (30 frames/h) are shown. Overlaid trajectories of cells shown in movie were detected and tracked using Fiji software.

Movie S6 (separate file)

Related to Figure 4. Representative video of JKX4$^{-/-}$-X4 cell migration on fibronectin-coated μ-Slide Chemotaxis chambers following a CXCL12 gradient on top. Images over time (30 frames/h) are shown. Overlaid trajectories of cells shown in movie were detected and tracked using Fiji software.

Movie S7 (separate file)

Related to Figure 4. Representative video of JKX4$^{-/-}$-R334X cell migration on fibronectin-coated μ-Slide Chemotaxis chambers in the absence of a CXCL12 gradient. Images over time (30 frames/h) are shown. Overlaid trajectories of cells shown in movie were detected and tracked using Fiji software.

Movie S8 (separate file)

Related to Figure 4. Representative video of JKX4$^{-/-}$-R334X cell migration on fibronectin-coated μ-Slide Chemotaxis chambers following a CXCL12 gradient on top. Images over time (30 frames/h) are shown. Overlaid trajectories of cells shown in movie were detected and tracked using Fiji software.

Movie S9 (separate file)

Related to Figure 7. Representative video of JKX4$^{-/-}$βarr$^{-/-}$-X4 cell migration on fibronectin-coated μ-Slide Chemotaxis chambers in the absence of a CXCL12 gradient. Images over time (30 frames/h) are shown. Overlaid trajectories of cells shown in movie were detected and tracked using Fiji software.

Movie S10 (separate file)

Related to Figure 7. Representative video of JKX4$^{-/-}$βarr$^{-/-}$-X4 cell migration on fibronectin-coated μ-Slide Chemotaxis chambers following a CXCL12 gradient on top. Images over time (30 frames/h) are shown. Overlaid trajectories of cells shown in movie were detected and tracked using Fiji software.

Movie S11 (separate file)

Related to Figure 7. Representative movie of CXCR4-AcGFP on live JKX4$^{-/-}$βarr$^{-/-}$-X4 cells captured by SPT-TIRF, showing the diffusion of CXCR4 particles (monomers, dimers, and nanoclusters) at steady state (FN). The video was acquired and displayed at 10 frames/s.

Movie S12 (separate file)

Related to Figure 7. Representative movie of CXCR4-AcGFP on live JKX4$^{-/-}$βarr$^{-/-}$-X4 cells captured by SPT-TIRF, showing the diffusion of CXCR4 particles (monomers, dimers, and nanoclusters) after CXCL12 stimulus. The video was acquired and displayed at 10 frames/s.

Movie S13 (separate file)

High-resolution representative movie of CXCR4-AcGFP on live JKX4$^{-/-}$-X4 cells captured by SPT-TIRF, showing the diffusion of CXCR4 particles (monomers, dimers, and nanoclusters) at steady state (FN). The video was acquired and displayed at 10 frames/s.

Movie S14 (separate file)

High-resolution representative movie of CXCR4-AcGFP on live JKX4$^{-/-}$-X4 cells captured by SPT-TIRF, showing the diffusion of CXCR4 particles (monomers, dimers, and nanoclusters) after CXCL12 stimulus. The video was acquired and displayed at 10 frames/s.

Movie S15 (separate file)

Single particle trajectories overlaid on representative movie S13.

Movie S16 (separate file)

Single particle trajectories overlaid on representative movie S14.

Supplementary Methods

Cells and reagents

HEK-293T cells were obtained from the American Type Culture Collection (CRL-11268 and CRL-10915, respectively). Jurkat (JK) $CD4^+$ cells were kindly donated by Dr. J. Alcamí (Centro Nacional de Microbiología, Instituto de Salud Carlos III, Madrid, Spain). We employed the CRISPR/Cas9 system to generate a JK cell line lacking CXCR4. We used the plasmid plFA1, which is a modified version of the pSpCas9n (BB)-2A-GFP (PX461) plasmid containing an additional cloning site for an sgRNA coding sequence, flanked by a hU6 promoter and a scaffold RNA coding sequence, kindly donated by Dr. R. M. Rios (1). This plasmid allows the expression of the Cas9n (nickase variant) protein and two sgRNAs, increasing the specificity and the efficiency of the mutagenesis process. Primers for targeting exon 2 of CXCR4 were designed and cloned into plFA1 using Crispr web tools from the Zhan laboratory (https://zlab.bio/guide-design-resources). The primers used to generate the sgRNA coding sequence targeting exon 2 of CXCR4 were CACCGAAGCATGACGGA CAAGTAC/AAACGTACTTGTCCGTCATGCTTC (for inclusion into the first site of plFA1) and CCGGTCTTCTGGTAACCCATGACC/AAACGGTCATGG GTTACCAGAAGA (for inclusion into the second site of plFA1). plFA1 containing the sgRNA coding sequences was used to electroporate JK cells using a BioRad electroporator (20×10^6 cells/400 μl RPMI 1640 with 10% fetal calf serum [FCS]; 975 μF and 280 V). Cells expressing the GFP reporter were selected after 48 hours using a cell sorter (FACSAria, BD Biosciences), pooled and maintained in culture (RPMI 1640 with 10% FCS at 37ºC and 5% CO_2). CXCR4 expression was analyzed by flow cytometry using an anti-human CXCR4-PE (12G5, Biolegend) (Supplementary Fig. 1a). Finally, CXCR4-deficient cells ($JKX4^{-/-}$) were isolated and cloned by limiting dilution and flow cytometry. The absence of CXCR4 in the selected clones was confirmed by analyzing their ability to migrate towards CXCL12 gradients in Boyden (Transwell) chambers (Supplementary Fig. 1b). We checked the mutated genomic region by sequencing a fragment of ~950 bp covering the targeted area that was amplified by PCR using the following primers: Fw 5´

ATGTGACTTTGAAACCCTCAGC 3´and Rv 5´ CCTTGGAGTGTGACAG CTTG 3´. PCR products were cloned into the pGEM-T vector and sequenced using SP6 and T7 primers.

When needed, JK cells were transiently transfected by electroporation with CXCR4-AcGFP or CXCR4^{R334X}-AcGFP (20 μg) (BioRad platform; as described). Cells were analyzed for GFP expression by flow cytometry 24 hours after transfection. For homozygous receptor expression, CXCR4-AcGFP (-X4) or CXCR4$^{-/-}$-AcGFP (-R334X) was transfected into JKX4$^{-/-}$ cells to generate JKX4$^{-/-}$-X4 or JKX4$^{-/-}$-R334X cells, respectively. For heterozygous receptor expression, the same constructs were transfected into JK cells to generate JK-X4 and JK-R334X cells, respectively.

Single molecule TIRF imaging and analysis

Cells were transiently transfected with the corresponding receptor fused to the AcGFP monomeric protein. Twenty-four hours after transfection, cells expressing low receptor-AcGFP^{+} levels were selected by cell sorting on a BD FACS Aria II SORP (BSL-2; Beckman Coulter) platform for detection and tracking analysis. CXCR4 expression levels were then evaluated using the Dako Cytomation Qifikit and flow cytometry as previously described (2, 3) and found ~8,500–22,000 receptors/cell, which equates to a density of <4.5 particles/μm^2. Cells were plated in complete medium for, at least, 2 hours (37ºC, 5% CO_2), and then resuspended in a buffer containing 25 mM HBSS, 25 mM Hepes, 2% FBS (pH 7.3) and plated on glass-bottomed microwell dishes (MacTec Corp.) coated with Fibronectin (Sigma Aldrich, 20 μg/ml, 30 min, 37ºC, 5% CO_2). When ligand effect was required, dishes were coated with CXCL12 (100 nM, 1h, 37ºC), and cells were incubated (20 min, 37ºC, 5% CO_2) before image adquisition.

Experiments were performed using a total internal reflection fluorescence (TIRF) microscope (Leica AM TIRF inverted) equipped with an EM-CCD camera (Andor DU 885-CS0-#10-VP), a 100× oil-immersion objective (HCX PL APO 100×/1.46 NA) and a 488-nm diode laser. The microscope was equipped with incubator and temperature control units; experiments were performed at 37ºC with 5% CO_2. To minimize photobleaching effects before image acquisition, cells were located and focused using the bright field, and a fine focus adjustment in TIRF mode

was made at 5% laser power, an intensity insufficient for single-particle detection that ensures negligible photobleaching. Image sequences of individual particles (500 frames) were then acquired at 49% laser power with a frame rate of 10 Hz (100 ms/frame). Penetration depth of the evanescent field was 90 nm. Video resolution depends on the requirements of the microscope (Supplementary Movies S13 and S14).

Particles were detected and tracked using previously described algorithms (U-Track2 implemented in MATLAB) (Supplementary Movies S15 and S16), as described (4). Mean spot intensity (MSI), number of mobile and immobile particles and diffusion coefficients ($D_{1\text{-}4}$) were calculated from the analysis of thousands of single trajectories over multiple cells (statistics provided in the respective figure captions), using described routines (5). Only tracks longer than 20 frames were used for further analysis; particles that merged or splitting and those located out of the cell body (filopodia) were excluded.

The minimum detectable diffusion coefficient in our experimental conditions was determined using purified AcGFP (monomeric) proteins immobilized on glass coverslips. We used < 0.0015 $\mu m^2/s$ as the threshold to discriminate between mobile and immobile trajectories, as this was the diffusion coefficient corresponding to 95% of the immobile AcGFP molecules.

Particle stoichiometry was determined by calculating the intensity value of each particle as a difference between particle intensity and the background in each frame. To minimize photon fluctuations within a given frame, we calculated the average value of particle intensity (background subtracted) over the first 20 frames (~2 s). To ensure that in this range of frames we didn't have photobleaching events, we measured photobleaching times from CD86-AcGFP on transiently transfected JK cells and quantitate only those particles that showed a unique single photobleaching step. Fitting of the distribution to a single exponential decay renders a T_o value of ~5 s which corresponds to 50 frames (100 ms/frame). The total number of receptors/particles was estimated by dividing the average particle intensity by the particle intensity arising from individual AcGFP molecules. The intensity emitted by an individual AcGFP was determined on JK cells electroporated with CD86-AcGFP (Supplementary Fig. 4a). Distribution of monomeric particles intensities was analyzed by Gaussian fitting rendering mean value of 980 ± 86 a.u. A similar

intensity value form the monomer was obtained for CXCR4-AcGFP particles showing a unique photobleaching step. Therefore, this value was used as the monomer reference to estimate the number of receptor-AcGFP molecules per particle (Supplementary Figure 4b-d).

FRET saturation curves by sensitized emission

HEK-293T cells were transiently transfected with a fixed amount of CXCR4-CFP or $CXCR4^{R334X}$-CFP (2 μg) and increasing amounts of CXCR4-YFP, $CXCR4^{R334X}$-YFP or HTR7-YFP (0.25–4.25 μg), as described (6). Emission light was quantified using the Wallac Envision 2104 Multilabel Reader (Perkin Elmer) equipped with a high-energy xenon flash lamp (donor: receptor fused to C-CFP, 8-nm bandwidth excitation filter at 405 nm; acceptor: receptor fused to YFP, 10 nm bandwidth excitation filter at 510 nm). To determine $FRET_{50}$ and $FRET_{max}$ values, curves were extrapolated from data using a nonlinear regression equation applied to a single binding site model, with a 95% confidence interval (GraphPad PRISM).

1. M. P. Gavilan, *et al.*, The dual role of the centrosome in organizing the microtubule network in interphase. *EMBO Rep.* **19** (2018).
2. P. Poncelet, F. George, T. Lavabre-Bertrand, Immunological detection of membrane-bound antigens and receptors. *Methods Immunol. Anal.* **6** (1993).
3. L. Martínez-Muñoz, *et al.*, CCR5/CD4/CXCR4 oligomerization prevents HIV-1 gp120IIIB binding to the cell surface. *Proc. Natl. Acad. Sci. U. S. A.* **111** (2014).
4. K. Jaqaman, *et al.*, Robust single-particle tracking in live-cell time-lapse sequences. *Nat. Methods* **5**, 695–702 (2008).
5. C. O. S. Sorzano, *et al.*, Image processing protocol for the analysis of the diffusion and cluster size of membrane receptors by fluorescence microscopy. *J. Vis. Exp.* **2019** (2019).
6. L. Martínez-Muñoz, *et al.*, Separating Actin-Dependent Chemokine Receptor Nanoclustering from Dimerization Indicates a Role for Clustering in CXCR4 Signaling and Function. *Mol. Cell* **70**, 106-119.e10 (2018).